Environmental Research Letters

LETTER • **OPEN ACCESS**

Monitoring the pendulum between El Niño and La Niña events

To cite this article: Jingzhi Su *et al* 2018 *Environ. Res. Lett.* **13** 074001

View the article online for updates and enhancements.

This content was downloaded from IP address 106.120.73.155 on 22/06/2018 at 01:45

Environmental Research Letters

LETTER

Monitoring the pendulum between El Niño and La Niña events

Jingzhi Su[1,5], Tao Lian[2], Renhe Zhang[3] and Dake Chen[4]

[1] State Key Laboratory of Severe Weather, Chinese Academy of Meteorological Sciences, Beijing, People's Republic of China
[2] State Key Laboratory of Satellite Ocean Environment Dynamics, Second Institute of Oceanography, Hangzhou, People's Republic of China
[3] Institute of Atmospheric Sciences, Fudan University, Shanghai, People's Republic of China
[4] State Key Laboratory of Satellite Ocean Environment Dynamics, Second Institute of Oceanography, Hangzhou, People's Republic of China
[5] Author to whom any correspondence should be addressed.

E-mail: sujz@cma.gov.cn

Keywords: ENSO pendulum, sea surface temperature, cluster

Supplementary material for this article is available online

OPEN ACCESS

RECEIVED
7 January 2018

REVISED
16 May 2018

ACCEPTED FOR PUBLICATION
16 May 2018

PUBLISHED
21 June 2018

Original content from this work may be used under the terms of the Creative Commons Attribution 3.0 licence.

Any further distribution of this work must maintain attribution to the author(s) and the title of the work, journal citation and DOI.

Abstract

The El Niño-Southern Oscillation (ENSO) pendulum swings back and forth between the El Niño and La Niña phenomena. To monitor the relative phase changes of the ENSO pendulum, 13 clusters are obtained based on the pattern of sea surface temperature anomalies (SSTAs) along the equatorial Pacific. The historical ENSO evolution can be effectively described by the alternation among those clusters. The zonal movement of SSTA loading during the ENSO evolution can also be captured by the changes in the clusters. One scheme was designed to monitor the ENSO pendulum based on those clusters as well the SSTAs in the Niño-3.4 region. When applied in practice to monitor historical ENSO events, including the 1997 El Niño and 2015 El Niño phenomena, the scheme tends be suitable for describing the ENSO pendulum between El Niño and La Niña, and it has the advantage of presenting both the ENSO amplitude and SSTA pattern.

1. Introduction

As the most significant interannual variability over the tropical Pacific, the El Niño-Southern Oscillation (ENSO) exerts dramatic impacts on the global climate Philander (1990). The warm ENSO phase is termed as El Niño, and the cold ENSO phase is termed as La Niña. ENSO swings back and forth between the two phases, which is referred to as the ENSO pendulum. The ENSO pendulum is usually represented by an index of regionally averaged sea surface temperature anomalies (SSTAs) in the Niño-3.4 region (5°N–5°S, 120°W–170°W). However, the ENSO cycle is not a standard pendulum but rather shows many irregular evolution features. The irregularity in the ENSO strongly challenges the ability to generate real-time ENSO predictions with a leading time of approximately two seasons or more (McPhaden *et al* 1998, Barnston *et al* 2012).

Extensive efforts have been made to discover the hidden regularity of the ENSO pendulum (Monahan and Dai 2004). In general, the El Niño phenomenon exhibits much more irregularity than the La Niña phenomenon (Kug and Ham 2011, Johnson 2013, Capotondi *et al* 2015). El Niño events can be classified into two types: the eastern-Pacific (EP) type, in which the maximum SSTA is in the cold tongue; and the central-Pacific (CP) type, in which the maximum SSTA is found near the equatorial date-line (Ashok *et al* 2007, Capotondi *et al* 2015). Studies have further proposed that extreme El Niño events should also be grouped into a specific type (Takahashi *et al* 2011, Chen *et al* 2015). However, such spatial diversity cannot be depicted by a single index, such as the Niño-3.4 index. Although many other indices have been proposed to scale the irregularity of the ENSO (Ashok *et al* 2007, Takahashi *et al* 2011, Ren and Jin 2011, Lian and Chen 2012, Capotondi *et al* 2015), determining the relative phase of certain SSTAs during the ongoing ENSO pendulum is difficult.

This study describes the evolution of the ENSO cycle by defining several empirical ENSO phases. As

© 2018 The Author(s). Published by IOP Publishing Ltd

will be shown, these ENSO phases can be naturally used to monitor both the ENSO pendulum and the zonal displacement of SSTAs associated with the ENSO. The dataset and methods are given in section 2. The results are shown in section 3. A summary and discussion are provided in section 4.

2. Dataset and method

SST data are obtained from the Extended Reconstructed Sea Surface Temperature version 5 (ERSSTv5) with a resolution of 2° × 2° (Huang *et al* 2017). The period of interest is 1950–2017, and the seasonal climatological mean was calculated based on the monthly SST data over the period from 1981–2010. Then, the entire monthly SSTA data of the whole period from 1950–2016 were used to conduct the clustering analysis without any detrending or filtering.

A method known as K-means clustering (Jain *et al* 1999) is applied to the equatorial Pacific SSTAs to derive the empirical phases of SSTAs. The strongest SSTA variabilities during the ENSO cycle are observed in the central-eastern equatorial Pacific; thus, the K-means clustering method is applied to the equatorial averaged SSTAs (5°N–5°S) within 170°E–90°W. The one-dimensional SSTAs are first smoothed with a moving window of 5 degrees along the equator. The K-means clustering is conducted with a measurement of the root-mean-squared Euclidean distance. The grouping number is set to 13 so that the positive and negative ENSO phases can be roughly divided into six phases and the neutral ENSO phase is represented by one prescribed phase. In practice, the neutral ENSO phase events are first selected with a restriction that all the amplitudes of SSTAs in the several Niño regions must be within one half of their standard deviation. The Niño regions include Niño-3 (5°N–5°S, 150°W–90°W), Niño-3.4, Niño-4 (5°N–5°S, 160°E–150°W), and equatorial Niño-1+2 (5°N–5°S, 90°W–80°W). Then, the warming ENSO phases are grouped into six clusters while the cold ENSO phases are grouped into another six clusters. The 13 clusters are sorted in ascending order based on their longitudinal average (170°E–90°W). Then the cluster index for each month is identified as the one with the minimum Euclidean distance between the 13 clusters and the one-dimensional equatorial SSTA of that given month. Our results are not sensitive to the SST datasets, cluster number, or longitudinal domains used (figures S15–S20; see the discussion in the supplementary information available at stacks.iop.org/ERL/13/074001/mmedia).

3. Results

3.1. Spatial pattern of the clusters

The longitudinal patterns of the 13 clusters are derived (figure 1(*n*)). The cluster with the largest label (C13) matches the peak of the super El Niño in which the longitudinal average is the maximum, etc. The longitudinal averages of the clusters from C1–C6 are negative and represent the negative phases of the ENSO pendulum. The clusters from C8–C13 represent the positive ENSO phases, in which the longitudinal average is positive. The longitudinal average of cluster C7 is approximately 0.02 °C. Therefore, cluster C7 can be interpreted as the neutral state.

Figures 1(*a*)–(*m*) show the SSTA patterns associated with the 13 clusters. Cluster C1 matches the strong La Niña patterns, and the centre of the minimum SSTA (approximately –1.7 °C) is located in the central equatorial Pacific (near 160°W). The negative centre of cluster C2 is located much further eastward in the eastern equatorial Pacific (around 110°W) and presents a weaker value of approximately –1.6 °C. For the negative clusters C3 and C5, the minimum centre is located in the central equatorial Pacific, whereas the centres of clusters C4 and C6 are located in the eastern equatorial Pacific.

The pattern of cluster C13 shows the prominent characteristics of super El Niños, which have strong SSTAs of approximately 3 °C located in the eastern equatorial Pacific. For cluster C12, although the SSTA reduces to approximately 2.4 °C, the maximum SSTA centre is still located in the eastern equatorial Pacific along with cluster C9. The maximum SSTA associated with cluster C11 is located in the central equatorial Pacific and has an amplitude of approximately 1.5 °C. The SSTA pattern associated with cluster C11 reflects the CP-type El Niño pattern, in which the maximum SSTA is located around 160°W. Such a CP-type El Niño pattern is also found in clusters C10 and C8 but with the centre of the maximum SSTA located further west (near the equatorial date-line).

3.2. Phase relationship of the clusters

The time series of the cluster index are compared with those of the SSTAs in Niño-3.4 (figure 2). Generally, the evolution of the cluster index is consistent with that of the Niño-3.4 index, and it has a correlation coefficient of 0.95. All the peaks of the Niño-3.4 index are precisely captured by the consistent cluster index, indicating that all the El Niño/La Niña events can be described by the cluster index. For example, the cluster C13 was observed during the peak phase of the super El Niño events of 1972, 1982, 1997, and 2015. For the CP El Niño events (1965, 1987, 1991, 1992, 1994, 2002, 2006, and 2009), their peak phases were consistent with that of cluster C11.

The cluster phases switch from one to another following the evolution of the ENSO cycle. The relationship of these clusters when they evolve from one to another within two consecutive months should be explored. The phase transition of these clusters can be clarified by the lead-lag relationship diagram (figures 3(*a*)–(*b*)). For example, the uppermost row of figure 3(*a*) indicates that one status of cluster C13 can only result from the one-month-leading cluster of C12

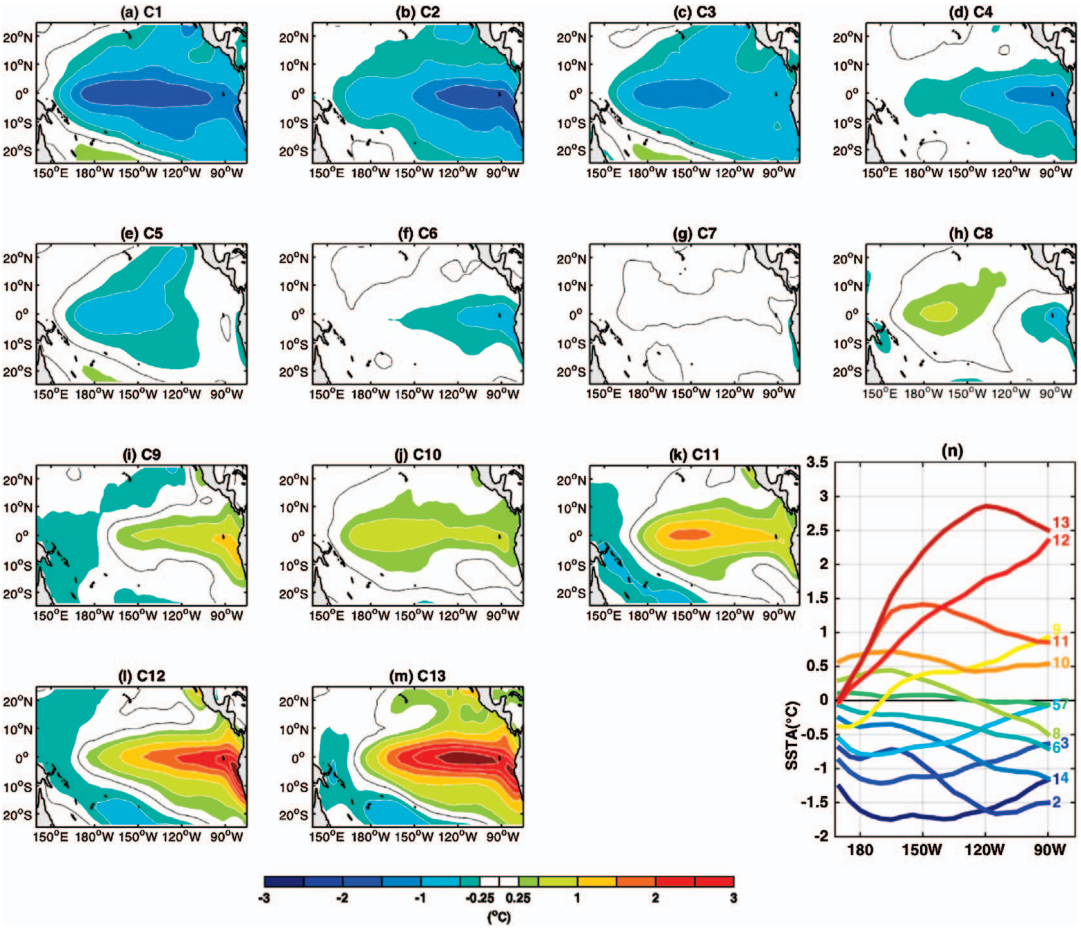

Figure 1. Composited SSTA pattern for each cluster ((*a*)–(*m*)) and equatorial average (5°N–5°S) of SSTA along the central-eastern equatorial Pacific for the 13 clusters (*n*). The 13 clusters are sorted in ascending order based on their longitudinal average.

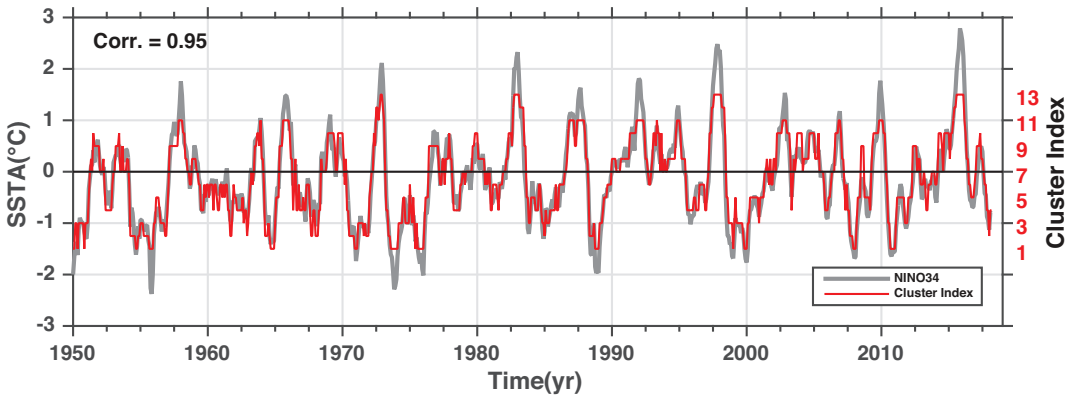

Figure 2. Time series of the cluster index (red line) and Niño-3.4 SST index (grey line).

(19%) or C13 (81%). The number in the parentheses indicates the transition probability. Inferred from the rightmost column of figure 3(*b*), one phase of cluster C13 may transfer into cluster C13 (81%), C12 (14%), or C11 (5%) in the next month.

Although cluster C11 may evolve into cluster C10 (21%), the transition from cluster C11 to C9 (EP-type) has seldom been observed (2%; the 11th column in figure 3(*b*)). Cluster C11 usually matches the peak of a CP-type El Niño (figure 2). During the decaying phase of the CP-type El Niño, the positive SSTAs associated with the CP-type El Niño generally persist locally in the central Pacific and decay westward (Kug *et al* 2009). Therefore, cluster C11 may readily evolve into a weaker CP-type El Niño phase of cluster C10 (figure 1). However, cluster C11 rarely transitions to cluster C9, in which the maximum SSTA is located in the eastern equatorial Pacific. On the other hand, cluster C11 may be transformed from a leading cluster of C12 (4%) or C9 (10%) centred in the eastern Pacific

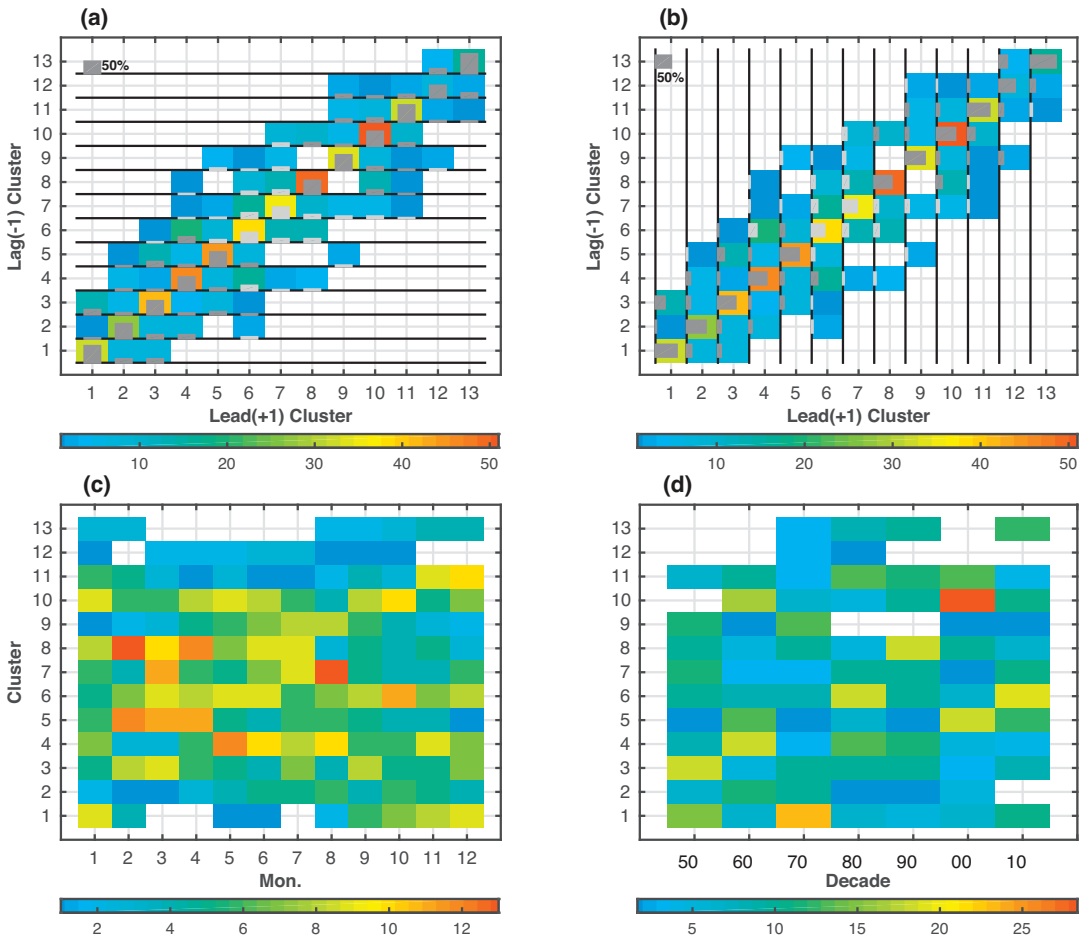

Figure 3. ((*a*)–(*b*)) Phase transition of the clusters between two consecutive months. (*c*) Number of clusters as the function of the calendar month. (*d*) Relative occurrence frequency (%) of clusters during each decade. In (*a*) and (*b*), the shading indicates the number of occurrences for each cluster. From the horizontal view of a row for certain cluster in (*a*), the origins of that cluster can be inferred, and their relative occurrence frequencies are indicated by grey bars. From the vertical view in (*b*), the column indicates the successor after each cluster, and their relative occurrence frequencies are indicated by grey bars. The events of the two consecutive months with a Niño-3.4 index within ±0.5°C are marked by grey-white bars, indicating that those events may be sensitive to classification due to the weak SSTA signals.

(the 11th row in figure 3(*a*)). The transformation from C12/C9 to C11 represents the westward movement of the SSTA centre from the eastern equatorial Pacific to the central equatorial Pacific, which will be further discussed in section 3.5. The CP-type cluster C11 mostly arises from a leading CP-type cluster of C10 at a relative probability of approximately 15%.

Generally, one cluster tends to keep its present phase with a larger relative probability (near or above 50%) than that in other cases to evolve into its neighbour clusters (figure 3(*b*)). Large uncertainties are found for clusters with lower longitudinal averages, such as cluster C6, C7 and C8, during which the Niño-3.4 index often falls within ±0.5 °C. A large diversity of ENSO evolution can emerge from this weak/neutral status.

3.3. Occurrence over seasonal and decadal time scales

Because the ENSO events tend to mature during the boreal winter, a few clusters show phase-locking features (figure 3(*c*)). Cluster C13 represents the peak of the super El Niño and tends to occur during the boreal autumn-winter, and it does not occur during the period from March to July. This phase-locking characteristic is consistent with the results of many previous studies (e.g. Rasmusson and Carpenter 1982, Tziperman *et al* 1997). Similarly, cluster C1, which represents the strong La Niña, also reaches a maximum in the boreal winter season.

On a decadal time scale, no strong El Niño events were observed during the 1950s, 1960s, and 2000s as indicated by the absence of cluster C12 and C13 over these periods (figure 3(*d*)). However, the 1982/83, 1997/98, 2015/16 El Niños and to a lesser extent the 1972/73 super El Niños explain the occurrence of C12 and C13 in the 1980s, 1990s, 2010s, and 1970s, respectively. Previous studies postulated that the ratio between the CP and EP El Niño increased in the 1990s and 2000s (Lee and McPhaden 2010, Newman *et al* 2011). This decadal variation can also be seen in figure 3(*d*). For example, the occurrence percentage of C8 and C10, which denote the CP El Niño type, is much higher in the 1990s and 2000s than in the other decades.

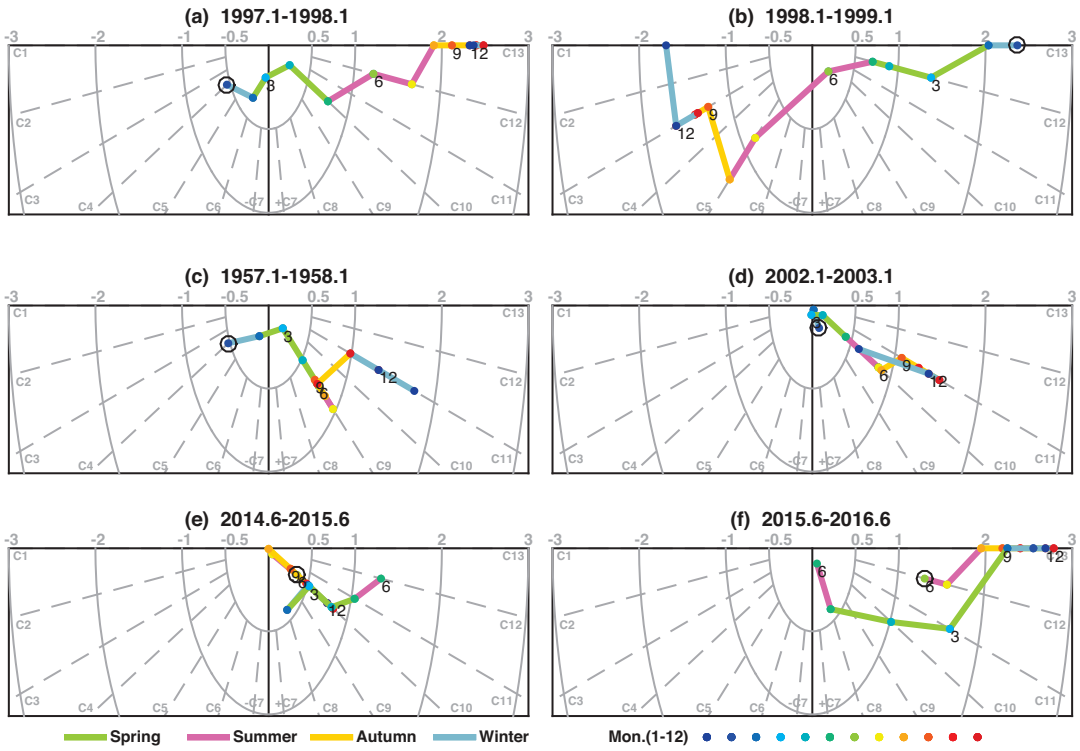

Figure 4. The ENSO pendulum monitored by cluster indexes for (*a*) 1997, (*b*) 1998, (*c*) 1957, (*d*) 2002, (*e*) 2014, and (*f*) 2015 ENSO events. The polar axis indicates the amplitude of the Niño-3.4 index, the polar angle indicates the cluster index. The time of those points are indicated by dots in different color for each month, and the seasons are indicated by lines in different color.

The occurrence of C11 after the 1990s corresponded to the CP-type El Niño of 1991/1992 and 1994 events and the three CP-type El Niños in 2002, 2006, and 2009/2010. The low frequency of C11 during the 2010s was caused by the 2015/2016 El Niño, which presented some CP-type patterns during its developing and decaying phase (Santoso *et al* 2017).

One notable feature is that the C8 cluster occurred during the 1990s with a higher frequency (figure 3(*d*)). From 1990–1994, several weak/moderate CP-type El Niño events occurred in the equatorial Pacific. As a result, the C8 cluster, which is featured in the weak CP-type El Niño, was frequently found in this period (figure 2; figure 3(*d*)). The high frequency of occurrence of the C8 cluster in this period also explains the strong self-persistence of the C8 cluster (more than 56%) in the phase transition diagram (figures 3(*a*)–(*b*)).

3.4. Pendulum of ENSO phases

To monitor the evolution of the ENSO, the cluster phases are plotted in polar coordinates (figure 4). The polar axis indicates the amplitude of Niño-3.4, and the polar angle indicates the cluster index. Hence, the left panel corresponds to cold phases while the right panel indicates warm phases. When the phase moves anticlockwise (from left to right), it may correspond with the developing phase of an El Niño in the right panel or the decaying phase of a La Niña in the left panel. Otherwise, if the phase moves clockwise, then one El Niño is decaying in the right panel or one La Niña is developing in the left panel.

The evolution of the 1997 El Niño event can be effectively described by the cluster phases in the ENSO pendulum (figure 4(*a*); figure S1). The Niño-3.4 index began to increase above 0.8 °C in May 1997, and the ENSO phase transferred into cluster C10 after April from the previous cluster of C7. As the Niño-3.4 index increased above 1.2 °C after June, the ENSO phase changed to C12 from June–July. The ENSO phase persisted in cluster C13 after August 1997 as the Niño-3.4 index increased above 2.0 °C afterwards.

The decay of the 1997 super El Niño began after February 1998. The ENSO pendulum began to turn clockwise after March 1998 (figure 4(*b*); figure S2) and was directed to cluster C12 during the spring of 1998. Then, the ENSO pendulum collapsed to cluster C9 in June 1998, with the Niño-3.4 index dropping to below zero. As the Niño-3.4 index quickly declined below approximately –0.7 °C after June 1998, the ENSO pendulum continued to turn clockwise and persisted in a phase of cluster C3 during September–December 1998. Finally, the ENSO pendulum turned to cluster C1, indicating an extreme La Niña event in 1998/1999. Thus, the developing and decaying features of the 1997/1998 El Niño can be well captured by the phase changes of the ENSO cluster as a pendulum.

3.5. Application of the ENSO pendulum

The clusters proposed here can also be used to show the zonal shift of the SSTA loading. During the ENSO evolution, the centre of the strong SSTAs may not be fixed locally to a certain region but may instead

move zonally. Such a zonal movement of SSTA loading, which is related with the intrinsic dynamics of ocean-atmosphere interactions, is an important feature of ENSO evolution.

The zonal shift of SSTA loading can be observed in the evolution of most El Niño events. For example, in the boreal spring of 1957, warm SSTAs first emerged in the far eastern Pacific along the west coast of South America (figure S3). The ENSO pendulum switched to cluster C9 (EP-type) in March 1957 (figure 4(*c*); figure S4) as the regional averaged SSTA warmed up to approximately 0.5 °C in the Niño-3 region (5°N–5°S, 90°W–150°W), and the Niño-3.4 index was approximately 0.4 °C. March to October, the SSTAs in Niño-3 were consistently warmer than those in the Niño-3.4 region, and the ENSO pendulum was fixed on a phase of C9. Concurrently, the warm SSTAs began to extend westward to the central equatorial Pacific during the boreal summer. The SSTAs in Niño-3.4 rose to above 1.0 °C in November 1957, and the SSTAs in the eastern equatorial Pacific remained at approximately 1.0 °C. Then, the ENSO pendulum shifted to cluster C11 (CP-type) from its previous phase of C9 (EP-type). The shift from cluster C9–C11 is evidence of the westward movement of SSTA loading from the eastern equatorial Pacific to the central equatorial Pacific. A similar shift from cluster C9–C11 also occurred in the development of the 1965 El Niño (figures S5 and S6), which is consistent with the westward movement of the SSTA loading from the eastern equatorial Pacific to the central equatorial Pacific.

The 1957 and 1965 El Niños can be classified as CP-type events, based on the SSTA patterns during their peak phase occurred in the boreal winter (figures S3 and S5). Compared with the westward movement of SSTAs during these CP-type El Niños, other CP-type El Niños, such as the 1994 (Su *et al* 2014) or the 2002, 2004, and 2006 El Niños, tended to develop locally in the central equatorial Pacific from their initiation to peak phase (figure 4(*d*); figures S7–S10). As the centre of SSTAs persisted in the central equatorial Pacific during the 2002 El Niño, the ENSO pendulum was locked in a phase of CP-type cluster C10 during the period from April to August 2002. As the SSTAs increased to approximately 1.2 °C in the Niño-3.4 region after October 2002, and the ENSO pendulum switched to cluster C11. Clusters C10 and C11 depict the CP-type El Niño (figure 1), and this swinging of the ENSO pendulum demonstrates that the 2002 CP-type El Niño was developed locally in the central equatorial Pacific. Similar swinging of ENSO pendulum can also be found during the 2006 El Niño (figures S9 and S10). Hence, the ENSO pendulum can present information about SSTA spatial patterns as well their changes during ENSO evolution.

3.6. ENSO pendulum of the 2014–2015 El Niño

Perhaps the most interesting application of the ENSO pendulum is associated with the evolution of the 2014–2015 El Niño (figures 4(*e*)–(*f*); figures S11–S13). The development of an anticipated strong El Niño event was hindered in the boreal summer of 2014 (Menkes *et al* 2014, Min *et al* 2015, Chen *et al* 2015, Hu and Fedorov 2016, Su *et al* 2018). The SSTAs in the Niño-3 region warmed up to above 0.5 °C, the SSTAs in the Niño-3.4 were approximately 0.5 °C after May 2014, and the ENSO pendulum turned anticlockwise from its former phase of C7–C10 in May 2014 (figure 4(*e*); figure S11). However, the warming in the central-eastern equatorial Pacific was hindered during the boreal summer of 2014. The SSTAs in Niño-3.4 dropped below 0.5 °C during the period of July–September 2014. This un-anticipated stalled warming event is argued to be caused by the lack of the westerly wind bursts in the western-central equatorial Pacific (Chen *et al* 2015, Hu and Fedorov 2016, Lian *et al* 2017) and the occurrence of a strong easterly wind surge in the central equatorial Pacific (Min *et al* 2015, Hu and Fedorov 2016). The stalling of the 2014 El Niño can be demonstrated by the ENSO pendulum, which was locked in a static phase of C10 during May–June and held back to C9, or C7 during the period of July–August. Although the ENSO pendulum rose up to C10 since September 2014, it fell back again to C8 after January 2015.

After March 2015, the SSTA warmed quickly in both the Niño-3 and Niño-3.4 regions (Lian *et al* 2017, Chen *et al* 2017, Paek *et al* 2017, Su *et al* 2018). The ENSO pendulum began to turn anticlockwise in March 2015 to become a CP-type C10 and then a Cluster C11 in May 2015. Then ENSO pendulum reached a high phase of C12 after June 2015, with warm SSTAs above 1.2 °C in the Niño-3.4 region (figure 4(*f*); figure S12). As the Niño-3.4 SSTAs warmed up to approximately 2.0 °C after August 2015, the ENSO pendulum jumped to a phase of C13.

The 2015 El Niño started to decay in January 2016, and the SSTA in Niño-3.4 dropped quickly to below 2.0 °C in March 2016. Following its almost linear reduction, the Niño-3.4 SSTAs reached close to zero in June 2016, and the ENSO pendulum turned consistently clockwise from a phase of C13 in January 2016 to a CP-type C11 in February-March 2016, a CP-type C10 in April 2016, and then a CP-type C8 in May–June 2016 (figure 4(*f*); figure S13). The evolution of the 2015/16 El Niño with a CP-type pattern during its developmental and decaying phases is consistent with the results of (Santoso *et al* 2017).

4. Conclusions and discussion

Based on the 13 cluster groups derived from the equatorial Pacific SSTAs, the relative phases of the ENSO pendulum are described. Those clusters reflect the different ENSO flavors of the SSTA spatial patterns, and they can capture the phase changes during the ENSO evolution. In practice, the one-dimensional SSTAs

along the equatorial Pacific can be obtained for a certain period (e.g. monthly in this study). Then, the present equatorial SSTAs can be classified as one of the 13 clusters by finding the minimum distance between the one-dimensional SSTA and those clusters. The empirical clusters should be determined in advance with a standard reference, which was derived based on the values over the period from 1981–2010 in this study.

Compared with the conventional index of ENSO monitoring, the one-dimensional clusters contain features of the SSTA spatial pattern along the equator. These patterns provide valuable information about the ENSO evolution. Particularly, the zonal movement of the SSTA loading along the equator is strictly related to the intrinsic dynamic processes of the ENSO. Hence, the ENSO pendulum, in a frame of equatorial SSTA clusters, has an advantage of showing the spatial evolution of the ENSO as well as its amplitude.

The clusters describe both the pattern and magnitude of SSTA associated with the ENSO; thus, the phase-relationship of the ENSO pendulum based on these clusters may provide some potential techniques for ENSO prediction. For example, we have found a similar year (2005/2006) to the present 2017/18 La Niña event (figure S14). The clusters remained in a weak warming state (cluster C8/C10) during the boreal spring of 2005, and a similar warming state was observed during the boreal spring of 2016. Then, the ENSO pendulum gradually switched to the neutral phase and then the negative phase after the summer, with clusters falling between C2 and C5 during the boreal autumn and winter in both cases. Since the ENSO turned out to be an El Niño event after the summer of 2006 (figures S9 and S10), one may speculate that the present 2017/18 La Niña status could continue to decay during the following summer and could perhaps develop into a warming phase of the ENSO pendulum. However, several key factors can influence the ENSO formation, such as westerly wind bursts (Chen *et al* 2015, Lian *et al* 2017) and subtropical Pacific SSTAs (Su *et al* 2018) in the late spring and early summer seasons. Hence, the final evolution of the present 2017/18 La Niña status in the future presents many uncertainties. Further investigations are also necessary to explore the intrinsic ENSO evolution dynamics from the perspective of the ENSO pendulum, and the underlying dynamics will undoubtedly benefit the prediction models.

Acknowledgments

The comments from the three anonymous reviewers provided valuable suggestions that helped improve the paper. This work is supported by the National Key R&D Program of China (2016YFA0600602), the National Natural Science Foundation of China (41776039, 41690121 and 41690120), and the Basic Research Fund of CAMS (2018Z006 and 2018Z007). NOAA_ERSST_V5 data were provided by the NOAA/OAR/ESRL PSD, Boulder, Colorado, USA and accessed at their Web site at www.esrl.noaa.gov/psd/.

ORCID iDs

Jingzhi Su https://orcid.org/0000-0003-2024-1883

References

Ashok K *et al* 2007 El Niño Modoki and its possible teleconnection *J. Geophys. Res.* **112** C11007
Barnston A G *et al* 2012 Skill of real-time seasonal ENSO model predictions during 2002-11: is our capability increasing? *Bull. Am. Meteorol. Soc.* **93** 631–51
Capotondi A *et al* 2015 Understanding ENSO diversity *Bull. Am. Meteorol. Soc.* **96** 921–38
Chen D *et al* 2015 Strong influence of westerly wind bursts on El Niño diversity *Nat. Geosci.* **8** 339–45
Chen L *et al* 2017 Formation mechanism for 2015/16 super El Niño *Sci. Rep.* **7** 2975
Hu S and Fedorov A V 2016 Exceptionally strong easterly wind burst stalling El Niño of 2014 *Proc. Natl Acad. Sci.* **113** 2005–10
Huang B *et al* 2017 Extended reconstructed sea surface temperature version 5 (ERSSTv5), upgrades, validations, and intercomparisons *J. Clim.* **30** 8179–205
Jain A K, Murty M N and Flyn P J 1999 Data clustering: a review *ACM Comput. Surv.* **31** 264–323
Johnson N C 2013 How many ENSO flavors can we distinguish? *J. Clim.* **26** 4816–27
Kug J S and Ham Y G 2011 Are there two types of La Niña? *Geophys. Res. Lett.* **38** L16704
Kug J S, Jin F F and An S I 2009 Two types of El Niño events: cold tongue El Niño and warm pool El Niño *J. Clim.* **22** 1499–515
Lee T and McPhaden M J 2010 Increasing intensity of El Niño in the central-equatorial pacific *Geophys. Res. Lett.* **37** L14603
Lian T and Chen D 2012 An evaluation of rotated EOF analysis and its application to tropical Pacific SST variability *J. Clim.* **25** 5361–73
Lian T, Chen D and Tang Y 2017 Genesis of the 2014–2016 El Niños events *Sci. Chi. Ear. Sci.* **60** 1589–600
McPhaden M J *et al* 1998 The tropical ocean-global atmosphere observing system: a decade of progress *J. Geophys. Res.* **103** 14169–240
Menkes C E *et al* 2014 About the role of westerly wind events in the possible development of an El Niño in 2014 *Geophys. Res. Lett.* **41** 6476–83
Min Q *et al* 2015 What hindered the El Niño pattern in 2014? *Geophys. Res. Lett.* **42** 6762–70
Monahan A H and Dai A 2004 The spatial and temporal structure of ENSO nonlinearity *J. Clim.* **17** 3026–36
Newman M, Shin S-I and Alexander M A 2011 Natural variation in ENSO flavors *Geophys. Res. Lett.* **38** L14705
Paek H, Yu J Y and Qian C 2017 Why were the 2015/2016 and 1997/1998 extreme El Niños different? *Geophys. Res. Lett.* **44** 1848–56
Philander S G 1990 *El Niño, La Niña, and the Southern Oscillation* (New York: Academic) p 289
Rasmusson E M and Carpenter T H 1982 Variations in tropical sea surface temperature and surface wind fields associated with the Southern Oscillation/El Niño *Mon. Wea. Rev.* **110** 354–84
Ren H L and Jin F F 2011 Niño indices for two types of ENSO *Geophys. Res. Lett.* **38** L04704
Santoso A, Mcphaden M J and Cai W 2017 The defining characteristics of ENSO extremes and the strong 2015/2016 El Niño *Rev. Geophys.* 55 1079–129

Su J *et al* 2018 Sea surface temperature in the subtropical Pacific boosted the 2015 El Niño and hindered the 2016 La Niña *J. Clim.* **31** 877–93

Su J, Li T and Zhang R 2014 The initiation and developing mechanisms of central Pacific El Niños *J. Clim.* **27** 4473–85

Takahashi K *et al* 2011 ENSO regimes: reinterpreting the canonical and Modoki El Niño *Geophys. Res. Lett.* **38** L10704

Tziperman E L, Zebial S E and Cane M A 1997 Mechanisms of seasonal-ENSO interaction *Atmos. Sci.* **54** 61–71